Fluid Motion and Heat Transfer in Autoignition Testing

Branson Davis[a] & Charline Fouchier[a,b] & Joseph Shepherd[a]

[a] Graduate Aerospace Laboratories, California Institute of Technology, Pasadena, CA, USA
[b] von Karman Institute for Fluid Dynamics, Sint Genesius Rode, Belgium

E-mail: *bdavis@caltech.edu*

Abstract

In this study, experimental measurements and three-dimensional numerical simulations were used to characterize the flow field inside our laboratories' Autoignition Temperature (AIT) facility based on the ASTM-E659 standard. Within the flask, small surface temperature differences, along with the downward movement of air through the center of the neck, create a single dominant toroidal vortex that transports fluid upwards along the walls and downward along the center line. Increasing the height of the flask holder caused the average temperature to increase and the magnitude/frequency of fluctuations to decrease. Studies of fuel-air mixing of ethene (C_2H_4), n-hexane (nC_6H_{14}), and n-dodecane ($nC_{12}H_{26}$) found that the lighter fuels more readily diffuse into air whereas the heavier fuels are more strongly influenced by buoyancy effects and take longer to mix. Further, in some cases the mixing time will be comparable to the time to ignition and long ignition times may result in significant quantities of fuel molecules escaping from the open top of the flask.

Keywords: *Thermal Ignition, Standardized Tests, Heat Transfer, Fluid Mechanics, Safety*

1 Introduction

The minimum autoignition temperature (AIT) of a fuel in hot air is used to evaluate the flammability and fire hazards of combustible gases and liquids. Early work to create standardized tests (Setchkin, 1954, Zabetakis et al., 1954)) has led the test methods which have evolved into the modern day ASTM-E659 (2005) standard in North America and its current international equivalent, ISO/IEC (2017). During an ASTM-E659 test, a small quantity of liquid fuel is injected into 500 mL flask containing hot air at atmospheric pressure. The AIT temperature is the minimum temperature for which ignition is observed within a limited time period in a series of trials varying the fuel amount and flask temperature following the procedure set out in the standard.

Many authors have since used the ASTM-E659 standards to characterize AITs for various liquid fuels. The reported AITs from extensive testing are tabulated in combustion safety databases, such as the Chemical Hazard Response Information System (CHRIS) and CHEMSAFE (Guard, 1999, Zakel et al., 2019). Recent experimental results of Martin and Shepherd (2021) emphasized that a wide range of ignition behaviors can occur, which could be categorized into at least four distinct modes. Measured AITs are also found to be sensitive to the specifics of the measurement technique, with variability often exceeding the precision of published data.

Recent experiments with our own ASTM-E659 apparatus indicate that the transient heat transfer and fluid motion inside the flask could significantly impact AIT measurements. The focus of this study is to investigate the effect various experimental setups conforming to the ASTM-E659 standards could have on the flow field inside the flask and temperature measurements used to report AITs. The temperature profile along the axis of symmetry inside the flask was characterized experimentally and compared with three-dimensional, unsteady numerical simulations. The influence of the mixing zone between outside air and the flask interior was identified as a key factor in determining the mean and fluctuating temperature profile in the flask. Numerical simulations of fuel-air mixing studies were conducted to characterize the transient mixing process that takes place after fuel is introduced into the flask.

2 Experimental Methods

For our study, we adapted the experimental setup used by Martin et al. for the characterization of the AITs for Jet A and surrogate jet fuels (Martin and Shepherd, 2021, Martin, 2023). This apparatus was constructed following the ASTM-E659 (2005) standard. Figure 1 shows a picture and a cross-section drawing of the setup.

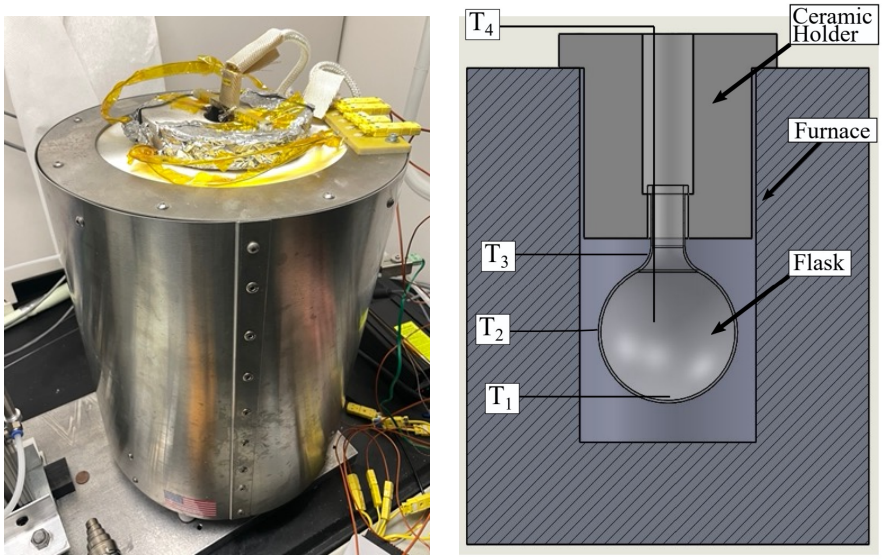

***Fig. 1**: Experimental apparatus*

The apparatus is composed of a Mellen CV12 crucible furnace with a 133 mm diameter and 200 mm deep cylindrical volume, which controllably heats up a 500 mL round bottom, borosilicate flask up to 1250 °C with a PID controller (Love Controls series 16B) system accurate to 1 °C. The flask is suspended in the furnace by a ceramic holder molded from silica-based Cotronics Rescor 750. The flask and ceramic holder are covered by aluminum foil to reflect the radiation inside the flask and reduce heat loss.

The temperature of the flask surface is measured with three 34 gauge, type K thermocouples inside a mineral-insulated metal sheath, set at positions T_1, T_2, and T_3 (see Figure 1). The thermocouple conventionally used to measure the air temperature, T_4, in ignition experiments was removed and replaced with a 36 gauge, type K thermocouple attached to a Velmex slide (NEMA 17, 155 mm travel) capable of precise vertical resolution. This allowed temperature measurements to be taken at various heights within the apparatus. The temperature variation is recorded with a NI 9213 16-channel, 24-bit, 75 Hz thermocouple data acquisition module from National Instruments, connected to a cDAQ-9171 CompactDAQ Chassis. We sampled each height for 120 s and waited an additional 120 s between measurements to allow unsteadiness effects caused by the movement of the internal thermocouple to dampen.

3 Numerical Methods

The transient, three-dimensional fluid motion, heat transfer, and mixing were numerically simulated by solving the Navier-Stokes equations of a multi-component ideal gas mixture. The equations of motion Eqn. (1)-(4), boundary and initial conditions were implemented in OpenFOAM using the PISO algorithm. We only considered non-reacting flow and did not attempt to model chemical reactions or the actual autoignition process in this study.

3.1 Geometric Model and Meshing

The flask and ceramic holder of the ASTM setup shown in Figure 1 were carefully measured and modeled in Solidworks to provide a suitable framework for simulation. The interior geometry was then meshed in three dimensions using the OpenFOAM tool, snappyHexMesh, prioritizing uniform hexahedral cells. A grid-independent solution, as determined from a statistical analysis of the unsteady flow, could be achieved for a grid of 6 million cells resulting in cell sizes of approximately 600 μm. In addition to modeling the flask and ceramic holder, a rectangular region above the flask (not shown in Figure 2) with open boundaries was included to model the exchange of gas between the flask and the surrounding atmosphere.

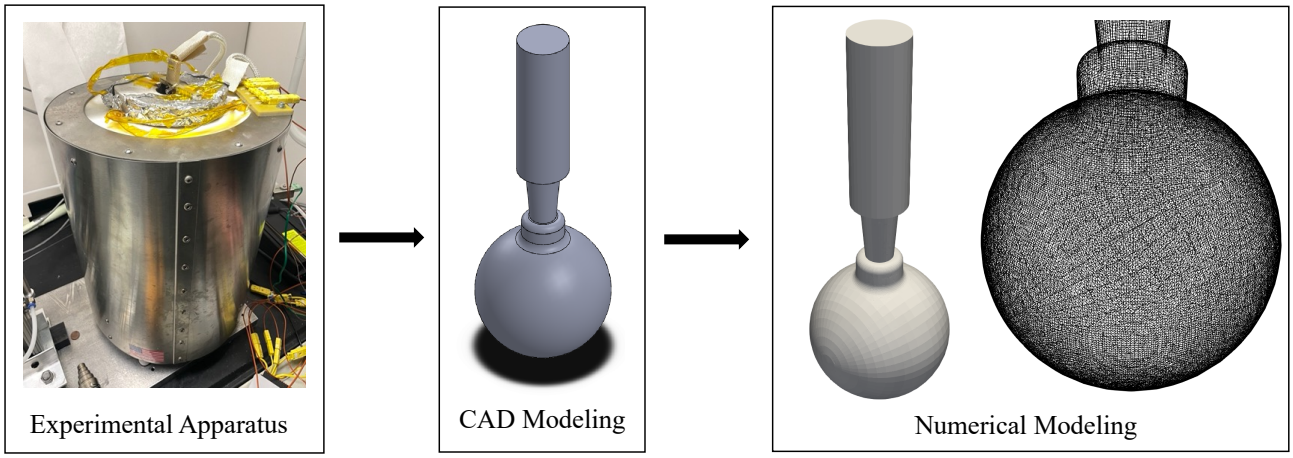

***Fig. 2**: Numerical Modeling of the ASTM apparatus*

3.2 Governing Equations

The governing equations we simulated were the variable-density Navier-Stokes equations for a Newtonian fluid with temperature-dependent transport properties and buoyancy forces in the momentum equation.

$$\frac{\partial \rho}{\partial t} + \nabla \cdot (\rho \mathbf{u}) = 0, \tag{1}$$

$$\frac{\partial}{\partial t}(\rho \mathbf{u}) + \nabla \cdot (\rho \mathbf{u}\mathbf{u} + p\mathbf{I}) = \nabla \cdot \tau + \rho \mathbf{g}, \tag{2}$$

$$\frac{\partial}{\partial t}(\rho Y_i) + \nabla \cdot (\rho Y_i \mathbf{u}) = -\nabla \cdot (\rho Y_i \mathbf{V}_i) \quad i = 1, 2, \ldots, K, \tag{3}$$

$$c_P \frac{\partial}{\partial t}(\rho T) + c_P \nabla \cdot (\rho \mathbf{u} T) = -\nabla \cdot (\lambda \nabla T) - \rho \nabla T \cdot \sum_{i=1}^{K} c_{P,i} Y_i \mathbf{V}_i, \tag{4}$$

where t is time, ρ is the mixture density, p is the pressure, u is the velocity, g is the acceleration due to gravity, T is the temperature, c_P is the specific heat at constant pressure, λ is the mixture thermal conductivity, Y is the mass fraction, $\mathbf{V}$ is the correction diffusion velocity, and τ is the viscous stress tensor written as:

$$\tau = \mu(\nabla \mathbf{u} + (\nabla \mathbf{u})^T) - \frac{2}{3}\mu(\nabla \cdot \mathbf{u})\mathbf{I} \tag{5}$$

where $\mathbf{I}$ is the identity matrix. The subscript, i, indicates the individual species, and K is the total number of species. For simulations in air, the species conservation equation and mass diffusion term

in the energy equation were omitted. The ideal gas equation of state was used to calculate the density of the mixture.

The diffusion velocities are calculated according to Chapman and Cowling (1990) using Fick's law, including a contribution by thermodiffusion (Soret effect) as:

$$\mathbf{V_i} = -\frac{D_i}{Y_i}\nabla Y_i - \frac{D_i \Theta_i}{X_i}\frac{1}{T}\nabla T \tag{6}$$

where X_i is the mole fraction, and Θ_i is the thermodiffusion ratio of species i. The individual-species mixture-averaged diffusion coefficients, D_i, are calculated according to Curtiss and Hirschfelder (1949) as:

$$D_i = \frac{1 - Y_i}{\sum_{j \neq i}^{N} \frac{X_i}{D_{ji}}} \tag{7}$$

where D_{ji} are the binary diffusion coefficients. To ensure the conservation of mass, a correction diffusion velocity is applied to $\mathbf{V}_i$ in Eqs (3) and (4) as described by Coffee and Heimerl (1981) as:

$$\mathbf{V}_i^C = \mathbf{V}_i + \mathbf{V}_C \, . \tag{8}$$

3.3 Initial and Boundary Conditions

Figure 3 shows the temperature boundary condition on the flask and holder as a function of height. A piece-wise linear profile in height z was imposed on the surface of the flask and was assumed constant in the holder section due to the large ceramic mass being held inside the furnace. These temperatures correspond to experimentally measured flask surface temperatures T_1, T_2, and T_3. A no-slip condition was imposed on the walls.

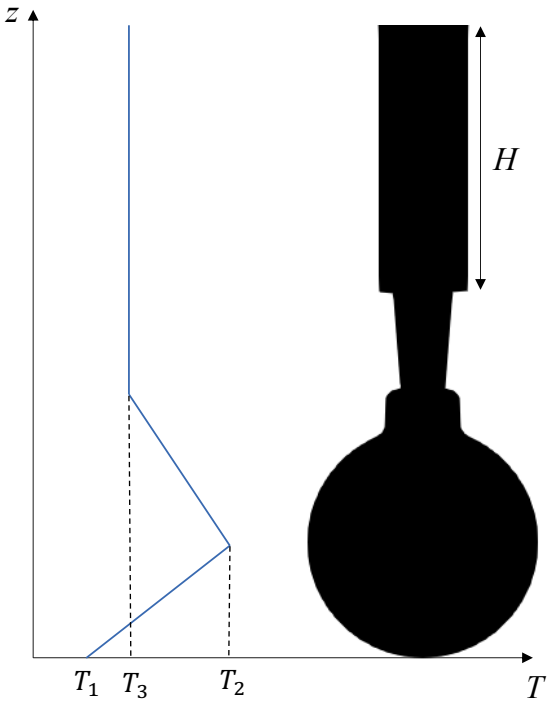

***Fig. 3**: Height-varying temperature boundary condition*

The simulations were initiated from rest at room temperature and continued until the temporal flow field became statistically stationary. Flow characterization and mixing simulations used this resultant flow field as an initial condition.

3.4 Test Conditions

The initial and boundary conditions were used to characterize a dry air flow field for various height ceramic holder pieces within the specs of the ASTM-E659 standard, which are summarized in Table 1. The inner diameter for all holders was 38.1 mm.

***Table 1**: Geometric holder configurations*

Case	Holder Height H (mm)
A	57.15
B	114.3
C	228.6

Case B corresponds to the dimension of the ceramic holders used in our laboratory and was used to numerically examine fuel mixing within the flask for gaseous ethene (C_2H_4), n-hexane (nC_6H_{14}), and n-dodecane ($nC_{12}H_{26}$). The ASTM-E659 standard with an open flask is intended for liquid or solid substances. Ethene was examined in order to investigate the effect of lighter, more diffusive fuels on the mixing process and efflux. Although the ASTM standard uses a closed flask for gas testing, the ISO/IEC (2017) international standard allows the testing of gas in an open flask similar to the ASTM liquid apparatus. The syringe injection process was not simulated, but instead, a 15 mm ball of fuel was initialized into a fully established flow field at the internal flask temperature. The resulting evolution of the composition (without reaction) was characterized as a function of time and space.

4 Results and discussion

4.1 Experimental Validation

To validate the numerical model, temperature measurements were digitally recorded and temporally averaged for a series of points on the vertical center line of the experimental apparatus and compared with values from the equivalent numerical simulation of case B. The position 0 mm corresponds to the bottom of the flask. Figure 4 (left) compares the average temperature between the experiment and the simulation. The vertical dashed lines indicate the top of the lower, spherical part of the flask (98 mm) and the upper neck of the flask (159 mm). A variation of 4 K was seen across the lower portion of the flask. Through the neck, a more significant 75 K temperature variation was seen due to the mixing region at the exit of the flask and within the ceramic holder. Above the flask, the temperature decreases with increasing height, approaching the value of the cold ambient air above the setup.

Comparing the average temperature between the simulation and the experiment within the lower part of the flask, the maximum deviation was only 1.5 K for any measured position. However, larger deviations in the temperature profile inside the ceramic holder can be observed. The surface temperature profile within the ceramic holder was not measured and was assumed to be spatially uniform in the simulation. This assumption is likely the source of discrepancy between simulation and experiment in this region.

Computed and observed temporal temperature fluctuations are shown in Figure 4 (right) at heights of 9, 47.1, and 159.5 mm along the flask center line. These heights correspond to the bottom, middle, and region immediately above the top of the flask. In the simulations, fluctuations up to 5 K are observed at the bottom of the flask and up to 12 K at the center of the flask. Immediately above the top of the flask, the flow is very unsteady. Fluctuations up to 80 K are observed with durations of approximately 0.1 s. The experimentally measured fluctuations for all heights are significantly less than those simulated, only 20 K at most above the flask in the ceramic holder. This difference is due to the slow response time of the thermocouple used for the measurements, estimated to have a characteristic step response time of $\tau = 1$ s to reach 67% of the final value. This is at least an order of magnitude slower than the fluctuations observed in the simulations and accounts for the observed differences.

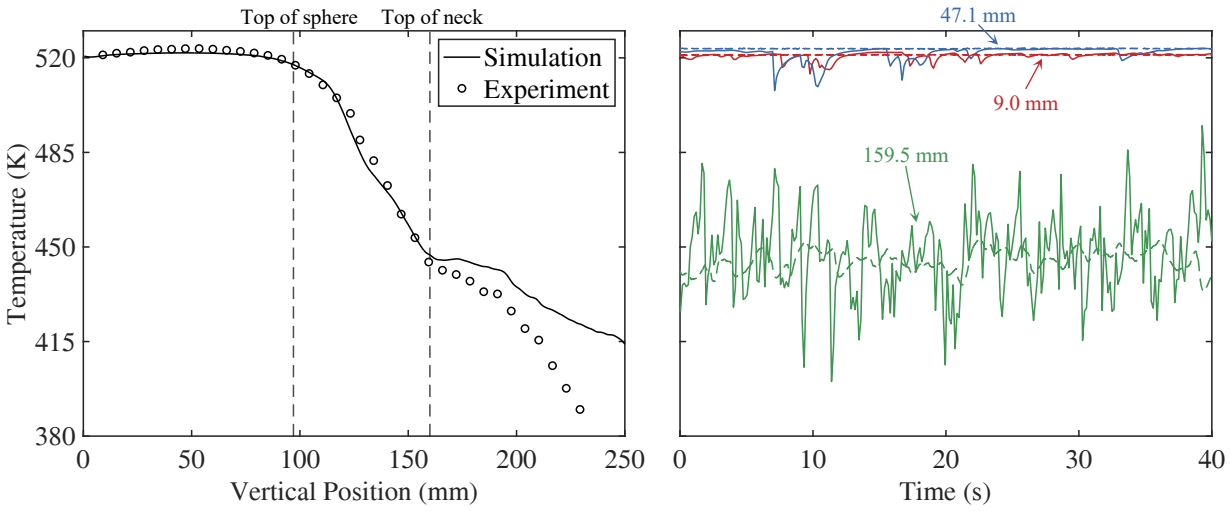

***Fig. 4**: (Left) Average temperature along the vertical center line of the flask, comparing simulation and experiment. (Right) Comparison of temperature fluctuations at selected heights between the simulation (solid lines, –) and experiment (dashed lines, - -)*

4.2 Effects of holder height

The ASTM standard allows users flexibility in the construction of the apparatus and in particular, the dimensions of the ceramic holder and the location of the flask within the furnace. We examined the influence of the three insulating holder heights shown in Table 1 on the fluid motion. The motion was simulated for 50 seconds after stationary statistics were achieved that were independent of start-up behavior. Figure 5 plots on a vertical cross-section through the center line the average temperature field and projected (surface) streamlines. For all three cases, a toroidal vortex is observed within the bottom of the flask. The flow is in the unsteady but laminar regime with an estimated Reynolds number (based on flask diameter and maximum center line gas velocity) of $Re \approx 120$. Flow is driven by both the temperature distribution in the flask and, more importantly, the flow of colder, more dense air penetrating down the ceramic holder through the center of the flask and an upward counterflow of hot air circulating from the bottom portion of the flask upward along the hot walls. Circulation cells commonly observed in natural convection flows within nonuniformly heated slots or cavities are observed above the flask within the ceramic holder. As the holder height is increased, the number of cells increases, from 2 to 10. The averaged flows are approximately axisymmetric but evidence of the three-dimensional motion and symmetry-breaking can be observed in the surface streamline patterns.

Examining the average temperature field, an unstable vertical stratification is apparent within the holder, with temperature decreasing with increasing height, as shown in Figure 6 (left). Modest variations in temperature can be observed within the round portion of the flask, case A was on average 7 K lower than case C. The temperature variations within the neck of the flask decrease with the increasing height of the ceramic holder. This is due to the increased mixing and longer residence time of the cold ambient gas as it plunges down through the longer holders into the flask. The cold air above the furnace has to travel further to reach the flask in case C compared to case A. The average downward velocity, Figure 6 (right), is lower in case C than in case A leading to a longer mixing time and greater heat transfer. Therefore, larger average temperatures are observed as the holder height increases. Transverse velocities along the center line (not shown) are two orders of magnitude smaller than the vertical component.

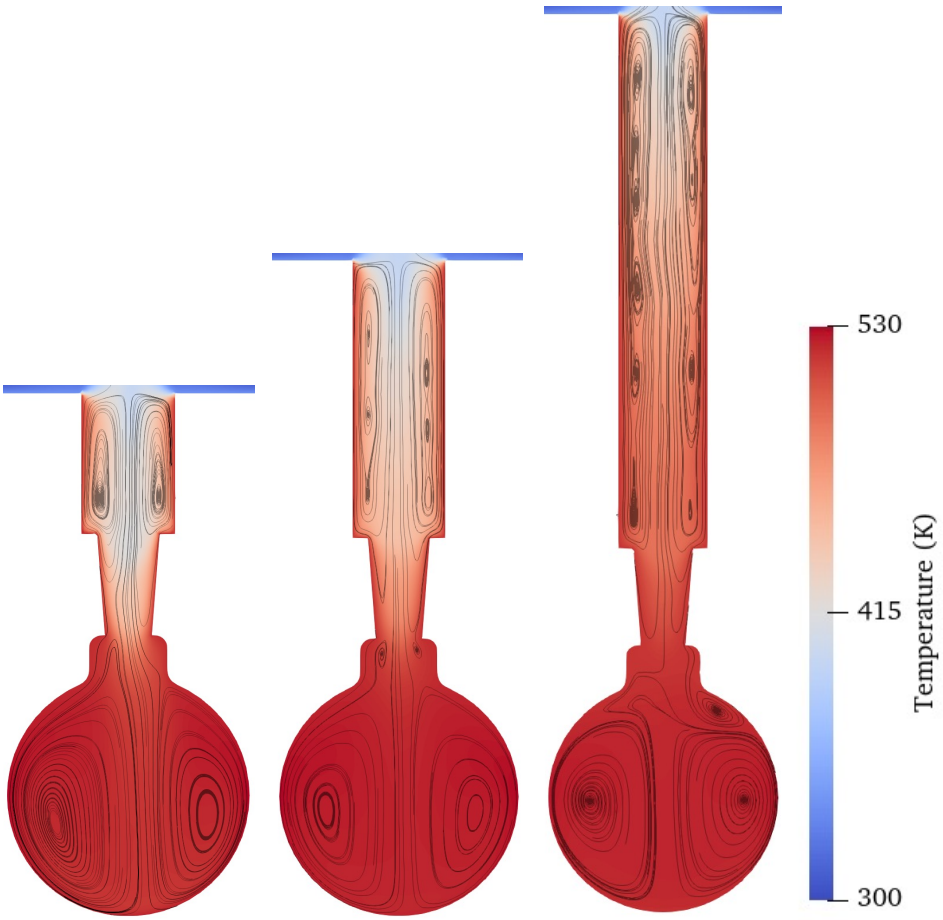

Fig. 5*: Average temperature field and surface streamlines along a vertical cross-section of the domain for the three holder heights*

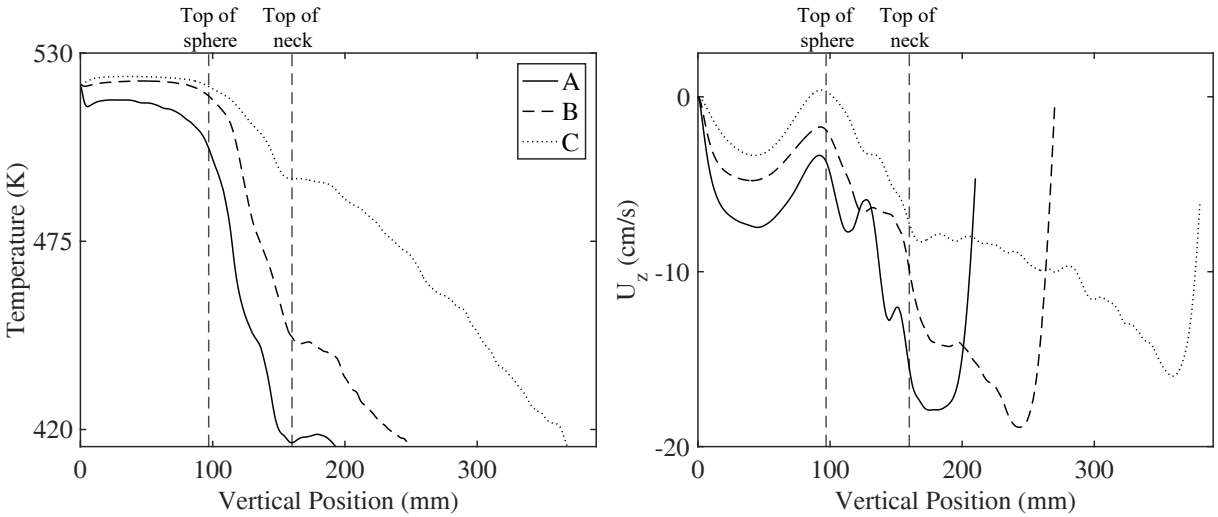

Fig. 6*: (Left) Average temperature profile and (Right) Average vertical velocity along the vertical center line for the three holder heights*

While averages can be informative about the large-scale features of the flow, temperature fluctuations[1] are important for unsteady reactive flow problems since reaction rates strongly depend on temperature.

[1] Correlations between temperature and composition and conditional averages of reaction rates are also important but we only examined non-reacting aspects of the flow in this study.

Table 2 gives the temporal temperature statistics in the center of the flask. This location is consistent with the nominal location of thermocouple T_4, used by the ASTM-E659 standard to monitor and characterize the temperature within the flask during ignition experiments. Case A had the largest temperature standard deviation (8 K) and largest absolute fluctuation size (38 K), while case C had the smallest standard deviation (0.9 K) and absolute fluctuation size (3 K). This is expected since the residence times of downward moving cold air are smaller in the shorter flask holder as compared to the taller holders.

***Table 2**: Statistical analysis of temperature at the center of the flask for the three holder heights*

Case	T_{avg} (K)	T_{std} (K)	T_{min} (K)	T_{max} (K)
A	515.6	8.00	477.2	522.1
B	520.6	3.30	494.3	523.6
C	522.8	0.90	519.7	524.1

The temporal average temperature was computed for all cells within the spherical portion of the flask. A histogram was obtained by binning the average temperature field. This is directly related to the probability distribution as the computational volumes are essentially identical in size and uniformly distributed. Figure 7 plots the distributions for the three holder heights. The location of the temperature at the center of the flask, T_4, is indicated with vertical lines. For the shortest holder, case A, the distribution is broadest, spanning 15 K, whereas cases B and C are narrower, spanning 9 and 8 K, respectively. These trends are consistent with the fluctuations reported in Table 2. With decreasing holder height, the flow fields become less steady and more cold air enters the flask, broadening the temperature probability distribution. For all holders, T_4 is on the left tail of their respective distributions with values of T_4 up to 5 K less than the median temperature. The implications for the reported AIT are discussed in Section 5.

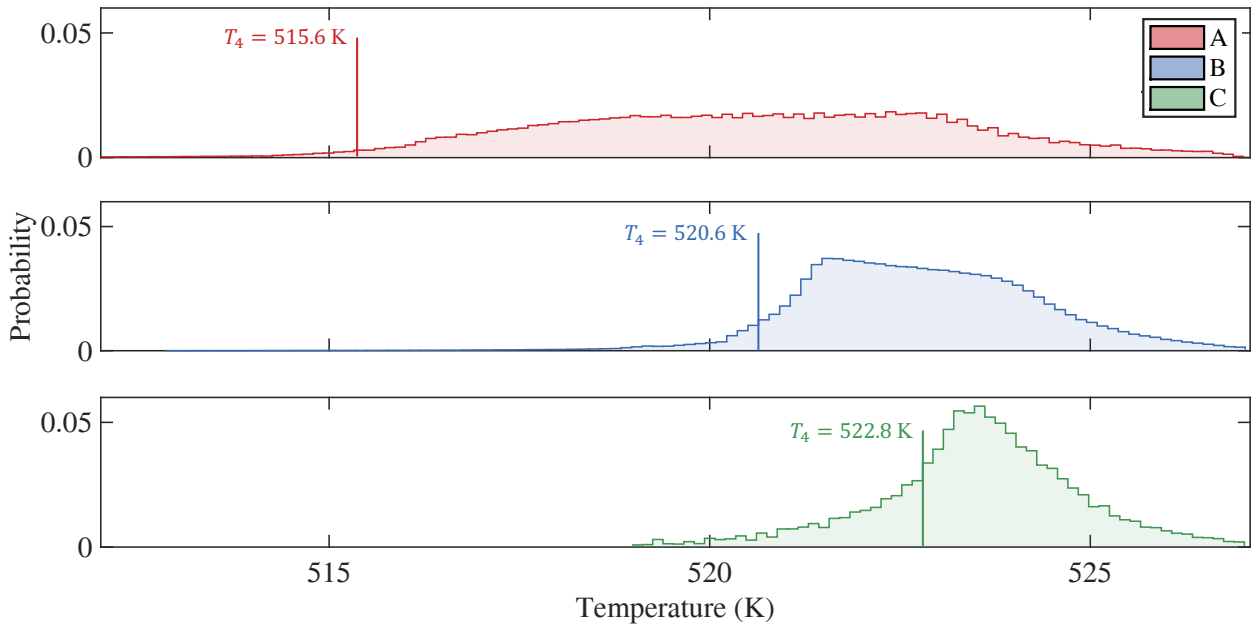

***Fig. 7**: Flask average temperature probability distributions for the three holder configurations. Flask center temperatures, T_4, are also indicated.*

4.3 Fuel Mixing

During an ignition experiment, fuel is injected from a syringe through a thin needle into the flask. Depending on the temperature, ignition can occur at a range of times following injection and with different extents of mixing depending on the fuel density and diffusivity. Understanding how the fuel distribution evolves within the flask following injection is also relevant to explaining the various modes of ignition that have been observed (Martin and Shepherd, 2021).

To study the effect of mixing, a ball of fuel in its gaseous phase was initialized near the bottom of the flask in an established dry air flow field. The temperature of the fuel sphere was set to be equal to the local air temperature at the time of injection. We acknowledge that a more complicated situation exists for liquid fuels, with droplets and two-phase mixtures emerging from the needle. The flow momentum, droplet vaporization, impact on the flask surface, and droplet dynamics, including the Leidenfrost effect, will influence the mixing behavior. Chemical reactions will also begin to take place concurrent with the mixing process. We have drastically simplified the problem to enable a preliminary analysis.

The evolution of fuel concentration over time was computed for three fuels of very different sizes and molecular weights. Figures 8 and 9 plot the mole fractions of C_2H_4 and nC_6H_{14} on a vertical cross-section through the center of the flask over time. The color bar is updated at every instance in time so that the mixing characteristics can be visualized. For the C_2H_4 case, the fuel initially rises slightly before being fully mixed in the flask within 30 seconds. The nC_6H_{14} and $nC_{12}H_{26}$ (not shown) cases mix very differently than C_2H_4. For the heavy molecules, the fuel initially sinks to the bottom of the flask before diffusing upwards and becoming fully mixed over a much longer period, 100-200 s.

The effect of varying the fuel molecular weight can be characterized by the density of the fuel sphere, ρ_F, the Froude number based on peak center line speed U, flask diameter d, and density normalized density difference $\Delta\rho/\rho_F = (\rho_F - \rho)/\rho_F$ between the fuel volume and surrounding air

$$Fr = \frac{U}{\sqrt{gd|\Delta\rho|/\rho_F}} \cdot \text{sign}(\Delta\rho_F)\,,$$

and the Schmidt number based on the mixture viscosity μ and fuel diffusivity D_F in the surrounding fuel-air mixture

$$Sc = \frac{\mu}{\rho D_F}\,.$$

Representative values for each fuel are shown in Table 3. Because all the cases were initialized at the same temperature and pressure, the initial density of the ethene sphere is slightly smaller than the ambient air density (0.69 kg·m^{-3}) and the initial density of the n-hexane and n-dodecane spheres are larger than ambient. As a consequence, Ethene is slightly buoyant with $Fr < 0$ and the flow is dominated by convection. The unstable fuel sphere is convected throughout the flask and the distorted volume rapidly mixes by diffusion. The n-hexane and n-dodecane are dominated by buoyancy with $1 \gg Fr > 0$. The initial negative buoyancy results in the fuel spheres settling to the bottom of the flask and then slowly diffusing upward with a stable interface between the fuel-air mixture and air.

***Table 3**: Molecular weight, Lennard-Jones parameter, fuel sphere density, Schmidt number, and Froude numbers for the three tested fuels*

Fuel	W_F [kg· kmol^{-1}]	σ_F [nm]	ρ_F [kg·m^{-3}]	Sc	Fr
C_2H_4	28	0.39	0.65	0.93	-0.27
nC_6H_{14}	86	0.59	2.00	1.8	0.059
$nC_{12}H_{26}$	170	0.76	3.95	2.6	0.053

The degree of "mixedness" can be studied to quantitatively assess how quickly the fuels mix within the flask. The intensity of segregation can be defined in terms of the coefficient of variation as described

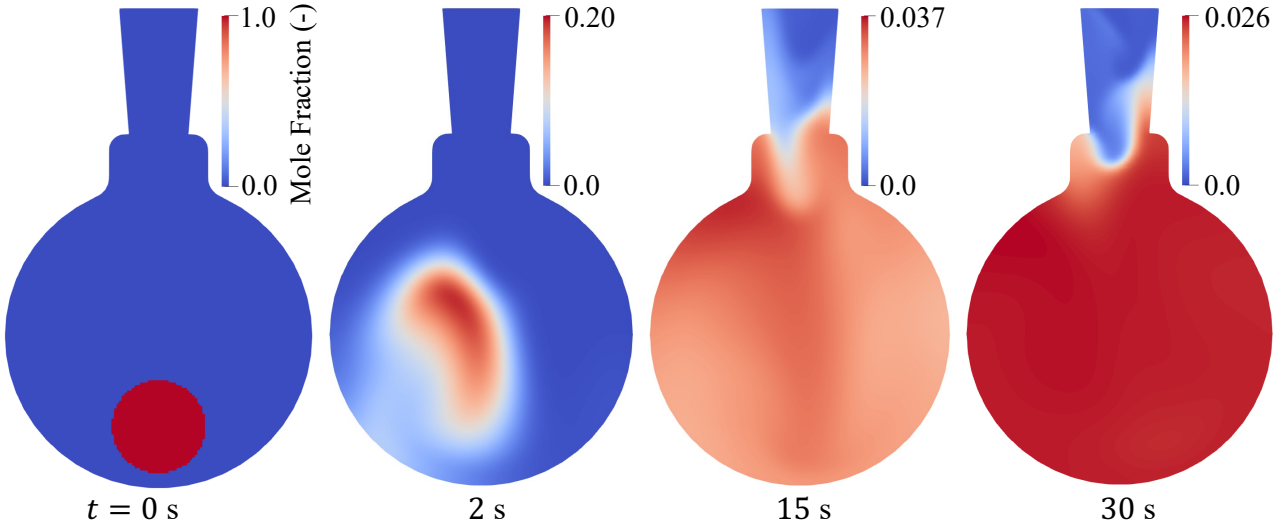

***Fig. 8**: C_2H_4 mole fraction temporal evolution on a vertical cross-section within the flask*

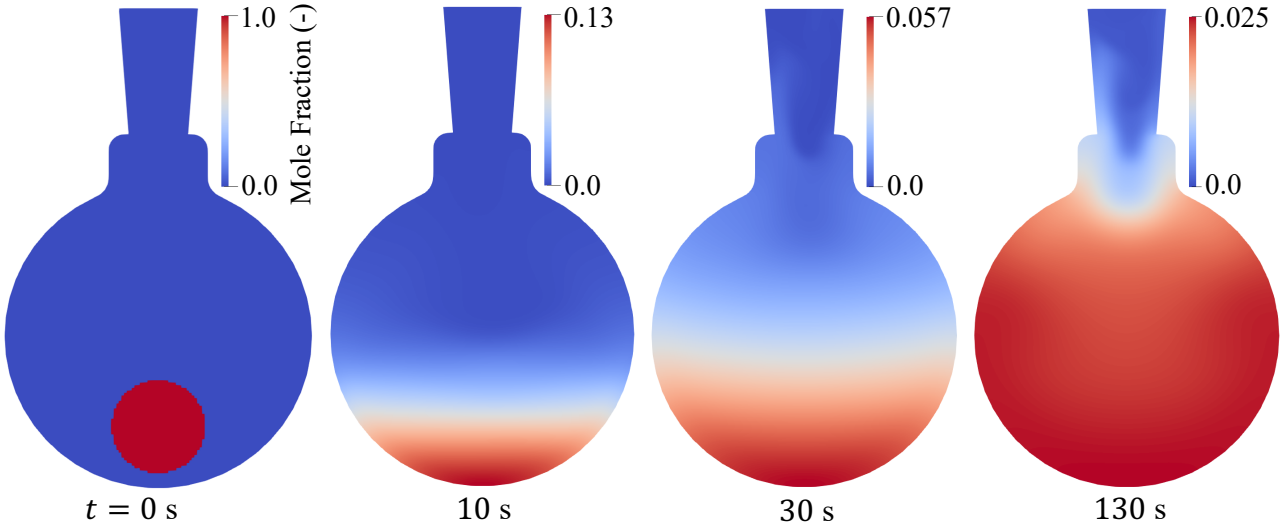

***Fig. 9**: nC_6H_{14} mole fraction temporal evolution on a vertical cross-section within the flask*

in Kukukova et al. (2009) as:

$$c_v = \sqrt{\frac{1}{N}\sum_{i=1}^{N}\left(\frac{X_i - \overline{X}}{\overline{X}}\right)^2} \tag{9}$$

where X_i is the fuel mole fraction for a given computation cell, $\overline{X}$ is the volume average fuel mole fraction, and N is the total number of cells in the domain. The coefficient of variation, c_v, can be normalized by the initial $c_v(0)$ to obtain a value between 0 and 1. Given that c_v computes the standard deviation over the mean, the value is largest for a perfectly unmixed state and will decay to 0 for a completely homogeneous mixture. As c_v is dimensionless, it can be readily compared between the different fuel cases. Figure 10 plots c_v against time for the three fuels. In very early times, the mixedness of n-hexane and n-dodecane decays more rapidly than ethene. This is caused by the strong buoyancy force that immediately drives the heavier fuels to the bottom of the flask. However, as time continues, ethene c_v reaches a steady value near zero significantly faster than for n-hexane and n-dodecane.

The effect of diffusivity on mixing can be understood by examining the estimated Schmidt numbers,

Sc, in Table 3. The increase in *Sc* with increasing fuel molecular weight is primarily due to the decrease in diffusivity with increasing fuel molecule size, although there is a small contribution (15%) from the difference in mixture kinematic viscosity. For example, consider how the binary diffusion coefficient (Kee et al., 2005) depends on both the molecular weights W_i and effective collision cross sections σ_{FA}^2

$$D_{FA} \propto \frac{1}{\sigma_{FA}^2}\sqrt{\frac{1}{W_F}+\frac{1}{W_A}}$$

where $\sigma_{FA} = (\sigma_F + \sigma_A)/2$ and σ_A = 0.35 nm. The increase in molecular size σ_F and decrease in diffusivity for the larger fuel molecules results in an increase in the time to mix, all other factors being the same. This accounts for the differences in the mixing rate of n-hexane and n-dodecane.

Taking a 5% level of c_v conventionally used in industry to characterize mixing time, the time to mix was = 11, 59, and 104 s for C_2H_4, nC_6H_{14}, and $nC_{12}H_{26}$, respectively. Previous work from Martin (2023) shows that nC_6H_{14} and $nC_{12}H_{26}$ can ignite before these times in some ASTM test conditions. In those cases, it is probable that ignition occurs before the fuel is fully mixed inside the flask.

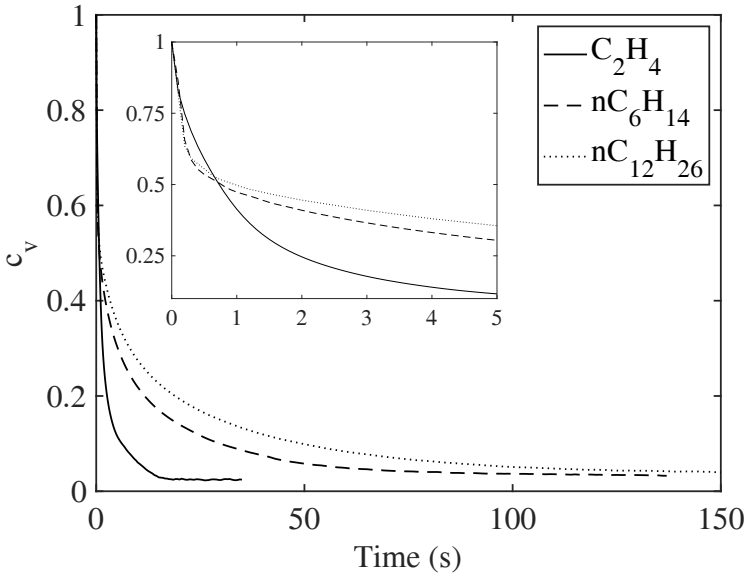

***Fig. 10**: Coefficient of variation (9) over time for C_2H_4, nC_6H_{14}, and $nC_{12}H_{26}$*

The number of fuel moles, *n*, within the flask can also be tracked over time by integrating spatially over the number of cells. This is shown in Figure 11. Since the same volume, pressure, and temperature were initialized, *n* is initially the same for all three cases. After 3 seconds, ethene molecules begin leaving the flask and the number of moles rapidly decreases over the next several seconds. After 26 s, 10% of the fuel has escaped into the holder and ambient air above. For n-hexane and n-dodecane cases, a 10% loss of fuel takes significantly longer at 117 and 173 s, respectively. The much slower loss of the larger, heavier fuel molecules is a consequence of the stable stratification, resulting in a much longer time for the fuel-air interface to reach the top of the flask, diffuse into the neck of the flask, and, ultimately, escape. For all cases, the time to lose 10% of the fuel molecules is longer than the time for the intensity of segregation to drop below 5%. Thus, the fuel molecules remain mostly within the flask prior to complete mixing, even for the smaller, lighter C_2H_4 case. Martin (2023) observed ignition of n-hexane and n-dodecane up to approximately 70 and 170 seconds, respectively. It's probable that less than 10% of the fuel leaves the flask before he observed ignition.

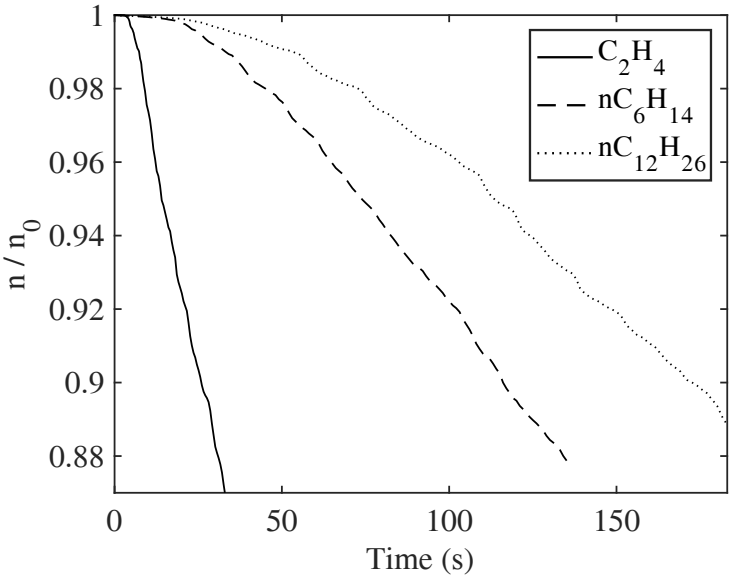

***Fig. 11**: Number of fuel moles normalized by the initial value within the flask over time*

5 Implications for AIT experiments

Our results (Figure 7) indicate that various setups, all conforming to the ASTM-E659 standard, can have significantly different temperature distributions. A range of temperatures can exist within the flask and will not be captured by the single point of measurement at T_4. Further, the size of fluctuations and general unsteadiness are different for the three cases we considered. This indicates that investigation and consideration of variations between apparatus construction is needed when evaluating reported results. The existence of a range of temperatures within the test flask indicates that care is needed in interpreting the values of AIT based only on the measurements of T_4.

We observe that fuel dispersion inside the flask is affected by the flow field and the fuel's physical properties, such as the density and diffusion coefficient. For short-duration tests, ignition could occur in a poorly mixed atmosphere before the fuel is perfectly dispersed, while for long-duration tests, loss of fuel could influence the AIT. Competing mixing and chemical timescales could cause AIT comparisons between different fuels to be misleading unless these factors are taken into account.

6 Conclusions

Experimental measurements and three-dimensional numerical simulations with realistic transport properties were used to characterize the flow field inside our ASTM E659 Autoignition Temperature (AIT) facility. Within the test flask, small surface temperature differences along with downward movement of air through the center of the neck create a single dominant toroidal vortex that transports fluid upwards along the walls and downward along the center line. Temperature measurements were made along the vertical center line in our AIT facility and were compared to a numerical simulation of the same geometry. A maximum variation of 4 K (0.7%) was observed in the average temperature within the flask. Above the flask, larger deviations between the simulation and experiment were observed due to the isothermal boundary condition used on the numerical model. For all measured locations, experimental temperature fluctuations were significantly smaller than those seen in the simulation at the same location, These discrepancies are attributed to the the slow response time of the thermocouple used in the experimental measurements.

A parametric study of the ceramic holder heights was carried out numerically to observe the effect on the resultant flow field. While the same toroidal vortex was seen within the bottom of the flask for all cases, the flow into the flask decreased and the number of convective cells seen on average increased with holder height. As a result, the average temperature for any given location along the vertical center line increased with increasing holder height. At the center of the flask, the average temperature for case A (shortest) was 7 K lower than for case C (tallest). Similarly, the absolute fluctuation size

decreased from 8 K with the shortest holder to 0.9 K for the tallest holder.

A parametric study was carried out to observe the effect of varying fuel molecule size and molecular weight on the mixing process within the flask. For the smallest molecule, ethene, complete mixing can occur in only 11 s due to minimal buoyancy effects and small Schmidt number. Heavier fuels, such as n-hexane and n-dodecane, consequently have much smaller, positive Froude numbers. Therefore, gravity initially plays a dominant role in forcing the fuel to the bottom of the flask. With significantly larger Schmidt numbers, these fuels diffuse much more slowly in air with mixing times of 59 and 104 s respectively, compared to ethene. A 10% loss of fuel molecules was observed after 25, 119, and 180 s for ethene, n-hexane, and n-dodecane, respectively. Therefore for all fuels studied, significant loss of fuel from the flask only occurs after complete mixing is obtained.

Our study has identified a number of factors that are important to consider in interpreting AIT data from the ASTM-E659 apparatus. We observe that both the construction of the apparatus (with the allowable specification of the standard) and the fluid motion induced by buoyancy can have a significant influence of gas inside the flask prior to ignition. The observed variability in temperature and fuel concentration may have an influence the measured autoignition temperatures and ignition delay times with implications for application to hazard assessment.

Acknowledgements

This research was carried out in the Explosion Dynamics Laboratory of the California Institute of Technology. This work was supported by The Boeing Company through a Strategic Research and Development Relationship Agreement CT-BA-GTA-1 and C. Fouchier was supported by the European Union through a Marie Sklodowska-Curie Fellowship.

References

ASTM-E659 (2005). *Standard test method for autoignition temperature of liquid chemicals*. American Society for Testing and Materials.

Chapman, S., Cowling, T. G. (1990). *The mathematical theory of non-uniform gases: an account of the kinetic theory of viscosity, thermal conduction and diffusion in gases*. Cambridge university press.

Coffee, T., Heimerl, J. (1981). *Transport algorithms for premixed, laminar steady-state flames*. Combust. Flame, 43:273–289.

Curtiss, C. F., Hirschfelder, J. O. (1949). *Transport properties of multicomponent gas mixtures*. J. Chem. Phys., 17(6):550–555.

Guard, U. C. (1999). *Chemical hazard response information system (chris)-hazardous chemical data*. Commandant Instruction, 16465.

ISO/IEC (2017). *ISO/IEC 80079-20-1: Explosive atmospheres - Part 20-1: Material characteristics for gas and vapor classification-test methods and data*. Technical report, International Organization for Standardization.

Kee, R. J., Coltrin, M. E., Glarborg, P. (2005). *Chemically reacting flow: theory and practice*. John Wiley & Sons.

Kukukova, A., Aubin, J., Kresta, S. M. (2009). *A new definition of mixing and segregation: Three dimensions of a key process variable*. Chemical engineering research and design, 87(4):633–647.

Martin, C. D. (2023). *Experiments in Thermal Ignition: Influence of Natural Convection on Properties of Gaseous Explosions*. Ph.D. thesis, California Institute of Technology.

Martin, C. D., Shepherd, J. E. (2021). *Low temperature autoignition of jet a and surrogate jet fuel*. Journal of Loss Prevention in the Process Industries, 71:104454.

Setchkin, N. P. (1954). *Self-ignition temperatures of combustible liquids*. Journal of Research of the National Bureau of Standards, 53(1):49.

The Open Foam Foundation (2023). *OpenFOAM*. `https://www.openfoam.org/`.

Zabetakis, M. G., Furno, A. L., Jones, G. W. (1954). *Minimum spontaneous ignition temperatures of*

combustibles in air. Industrial & Engineering Chemistry, 46(10):2173–2178.
Zakel, S., Brandes, E., Schröder, V. (2019). *Reliable safety characteristics of flammable gases and liquids–the database chemsafe*. Journal of Loss Prevention in the Process Industries, 62:103914.